Eur. J. Mineral.
2017, **29**, 295–306
Published online 5 April 2017

Cyprine, $Ca_{19}Cu^{2+}(Al,Mg,Mn)_{12}Si_{18}O_{69}(OH)_9$, a new vesuvianite-group mineral from the Wessels mine, South Africa

TARAS L. PANIKOROVSKII[1,*], VLADIMIR V. SHILOVSKIKH[2], EVGENIA Yu. AVDONTSEVA[1], ANDREY A. ZOLOTAREV[1], IGOR V. PEKOV[3], SERGEY N. BRITVIN[1], ULF HÅLENIUS[4] and SERGEY V. KRIVOVICHEV[1,5]

[1] Department of Crystallography, Saint-Petersburg State University, University Emb. 7/9, 199034 St. Petersburg, Russia
*Corresponding author, e-mail: taras.panikorovsky@spbu.ru
[2] Department of Colloidal Chemistry, Institute of Chemistry, Saint-Petersburg State University, University Av.26, 198504 St. Petersburg, Russia
[3] Department of Mineralogy, Moscow State University, Vorobievy Gory, 119991 Moscow, Russia
[4] Department of Geosciences, Swedish Museum of Natural History, Box 50007, 104 05 Stockholm, Sweden
[5] Institute of Silicate Chemistry, Russian Academy of Sciences, Makarova Emb. 6, 199034 St. Petersburg, Russia

Abstract: Cyprine, ideally $Ca_{19}Cu^{2+}(Al,Mg,Mn)_{12}Si_{18}O_{69}(OH)_9$, was found at the Wessels mine near Hotazel, Kalahari Manganese Field, North Cape province, South Africa. It occurs as chaotic aggregates (up to 5 cm across) in open cavities or embedded in coarse-grained colourless calcite. Associated minerals are calcite, apatite, andradite, henritermierite and rhodochrosite. Single crystals of cyprine up to 1 cm are dark red with a lilac hue and vitreous lustre. Dominant crystal forms are {1 0 0}, {1 1 0} and {3 3 1}. The Mohs hardness is 6.5. D_{meas} and D_{calc} are 3.40(3) and 3.41 g/cm^3, respectively. Cyprine is optically uniaxial, negative, $\omega = 1.744(2)$, $\varepsilon = 1.732(2)$ (in white light). Pleochroism is strong; ranging from *O* = dark purple, *E* = pale red to *O* = dark reddish brown, *E* = pale yellowish brown; $O \gg E$. Chemical composition (electron microprobe, H_2O by thermogravimetric analysis (TGA)) of two chemically different zones (zone-1/zone-2, wt.%) is: SiO_2 36.98/36.51; Al_2O_3 14.98/13.70; CaO 36.70/36.18; MgO 3.24/1.10; Mn_2O_3 2.27/6.04; CuO 2.39/1.86; Fe_2O_3 0.62/2.50; Cr_2O_3 0.23/0.04; H_2O 3.30/3.30, total 100.71/101.23. The crystal-chemical formulae (based on the FTIR, TGA/differential scanning calorimetry, SREF, WDS and optical spectra) are $Ca_{18.00}Ca_{1.00}(Cu_{0.95}Mg_{0.05})_{\Sigma 1.00}Al_{4.00}(Al_{5.50}Mg_{1.00}Mn^{3+}_{1.19}Fe^{3+}_{0.22}Cr_{0.09})_{\Sigma 8.00}([SiO_4]_{9.91}[H_4O_4]_{0.09})_{\Sigma 10.00}[Si_2O_7]_4((OH)_9O)_{\Sigma 10.00}$ and $Ca_{18.00}Ca_{1.00}(Cu_{0.90}Mg_{0.10})_{\Sigma 1.00}(Al_{3.22}Mn^{3+}_{0.60}Fe^{3+}_{0.18})_{\Sigma 4.00}(Al_{4.72}Mn^{3+}_{1.20}Fe^{3+}_{1.06}Mn^{2+}_{0.60}Mg_{0.40}Cr_{0.02})_{\Sigma 8.00}([SiO_4]_{9.91}[H_4O_4]_{0.09})_{\Sigma 10.00}[Si_2O_7]_4((OH)_9O)_{\Sigma 10.00}$ for zone-1 and zone-2, respectively. Absorption bands in the IR spectrum are 443, 490, 574, 604, 671, 814, 905, 972, 1015, 3354, 3640 cm^{-1}. The polarized optical absorption spectra have two strong absorption bands at 415 and 555 nm and a less intense band at 645 nm. The eight strongest lines of the powder X-ray diffraction pattern are (*I*–*d*(Å)–*h k l*): 12–5.89–0 0 2, 12–3.007–4 3 1, 47–2.950–0 0 4, 100–2.75–4 3 2, 76–2.594–5 2 2, 35–2.459–6 2 0, 10–2.324–1 4 4, 28–1.6224–6 7 2. Cyprine is tetragonal, space group *P*4/*n*, unit-cell parameters refined from the powder data are $a = 15.5652(5)$, $c = 11.7921(4)$, $V = 2863.2(2)$ Å^3, $Z = 2$. The crystal structure has been refined to $R_1 = 0.034$ and $R_1 = 0.035$ for 2848 and 2071 unique observed reflections with $|F_o| \geq 4\sigma_F$ for the zones 1 and 2, respectively. The structure refinements provide scattering factors of the *Y*1A,B sites close to 29 e^-, which supports occupancy of these sites by Cu^{2+} ions. The copper coordination polyhedra possess strong Jahn–Teller distortion: *Y*1A–O6(4×) = 2.043(3) Å and *Y*1A–O10 = 2.258(6) Å for zone-1 and *Y*1B–O6(4×) = 2.010(4) Å and *Y*1B–O10 = 2.274(7) Å for zone-2. Cyprine is defined as a member of the vesuvianite group with Cu^{2+} as a dominant cation in the *Y*1 site. The historical name cyprine (derived from Latin *cuprum*, copper) given by J.J. Berzelius in 1821 for Cu-bearing vesuvianite is transferred to the new mineral.

Key-words: cyprine; new mineral; Berzelius; optical spectra; IR; TGA/DSC; crystal structure; vesuvianite; copper; Wessels mine; South Africa.

1. Introduction

The vesuvianite group presently contains four mineral species: vesuvianite itself $Ca_{19}(Al,Mg,Mn,Fe)_{13}Si_{18}O_{68}(OH,F,Cl,O)_{10}$ (Werner, 1795), wiluite $Ca_{19}(Al,Mg,Fe,Ti)_{13}(B,Al,\square)_5Si_{18}O_{68}(O,OH)_{11}$ (Groat *et al.*, 1998), fluorvesuvianite $Ca_{19}(Al,Mg,Mn,Fe)_{13}Si_{18}O_{68}(F,OH)_{10}$ (Britvin *et al.*, 2003) and manganvesuvianite $Ca_{19}Mn^{3+}(Al,Mn^{3+},Fe^{3+})_{10}(Mg,Mn^{2+})_2Si_{18}O_{69}(OH)_9$ (Armbruster *et al.*, 2002). The simplified formula of vesuvianites, which have domain structure, hydrogarnet-type substitutions and different cation coordinations, may be written as $X_{18}X4Y1Y2_4Y3_8T_{0-5}[(ZO_4)_{10-x}(H_4O_4)_x](Z_2O_7)_4(OH,O)_{10-11}$ where $x < 3$, *X* are seven- to nine-coordinated sites, *X*4 has a square antiprism coordination, *Y*4 has a square pyramidal coordination, *Y*2 and *Y*3 have octahedral coordinations, T_{0-5} is the additional site with triangular and tetrahedral coordination, ZO_4 and Z_2O_7 are tetrahedral and ditetrahedral groups, respectively (Warren & Modell, 1931; Machatschki, 1932; Coda *et al.*, 1970;

DOI: 10.1127/ejm/2017/0029-2592
0935-1221/17/0029-2592 $ 5.40

Groat *et al.*, 1992; Armbruster & Gnos, 2000c; Galuskin *et al.*, 2003a). The vesuvianite structure has a pronounced rod-like organization along the fourfold axis. These rods are occupied by the *Y*1A,B (*Y*1) and *X*4A,B (*X*1) sites located at the various *z* levels. They have the *Y*1A–*X*4A–*X*4B–*Y*1B sequences with distances lower than 1.3 Å, 1.3 Å and 2.5 Å between the *Y*1A–*X*4A, *Y*1A–*X*4A and *X*4A–*X*4B positions, respectively, which leads to different ordering schemes and, as a result to different tetragonal space groups (Giuseppetti & Mazzi, 1983; Fitzgerald *et al.*, 1986b; Allen & Burnham, 1992; Pavese *et al.*, 1998; Armbruster & Gnos, 2000a and c).

It has long been known that vesuvianite may contain significant amount of copper: a blue vesuvianite from Sauland (Norway) was described by Jacob Berzelius in 1820 and named 'cyprine' from Latin *cuprum*, copper (Berzelius, 1821). Lindström (1890) investigated chemical compositions of some Norwegian vesuvianites and demonstrated that 'cyprine' contains only 0.73 wt.% CuO. Chemistry and crystal structure of 'cyprine' from the Franklin mine, Franklin, New Jersey, USA, was studied by Shannon (1922) and Fitzgerald *et al.* (1986a), who proposed that Cu preferentially occupies the *Y*1 site. The EXAFS investigations by Ohkawa *et al.* (1992) confirmed fivefold coordination of the Cu atoms in Cu-bearing vesuvianites. Electron paramagnetic resonance study (Dyrek *et al.*, 1992) of Norwegian 'cyprine' revealed local square environment of the Cu^{2+} ions, in agreement with the square-pyramidal coordination of copper at the *Y*1 site.

By virtue of the very high degree of structural complexity (Krivovichev, 2013), exceptionally complex chemical composition (Groat *et al.*, 1992), diversity of mechanisms of cation substitution and ordering in the vesuvianite group, its several members can potentially be defined as new mineral species (Ohkawa *et al.*, 1992; Armbruster & Gnos, 2000a and b; Armbruster *et al.*, 2002; Bellatreccia *et al.*, 2005 and references therein).

Cyprine (IMA2015-044) is a new vesuvianite-group mineral with predominance of Cu^{2+} at the *Y*1A,B sites. Its simplified formula is $Ca_{19}Cu^{2+}(Al,Mg,Mn)_{12}Si_{18}O_{69}(OH)_9$. Both the new mineral and its name have been approved by the Commission on New Minerals and Mineral Names of the International Mineralogical Association. The holotype specimen is deposited at the Mineralogical Museum of the Department of Mineralogy, St. Petersburg State University, St. Petersburg, Russia (catalogue number 1/19652).

2. Occurrence

Cyprine was found at the Wessels mine, near Hotazel, Kalahari Manganese Field, North Cape province, South Africa (Cairncross *et al.*, 1997), in association with calcite, apatite, andradite, henritermierite and rhodochrosite. The mineral has a hydrothermal origin. The assemblage containing cyprine and associated Mn- and Ca-bearing minerals was formed as a result of the hydrothermal activity (Kleyenstuber, 1984; Dixon, 1989). The main hydrothermal event that led to enrichment of the Mn ore has been dated with sugilite at 1048 ± 5.9 Ma (Gnos *et al.*, 2003).

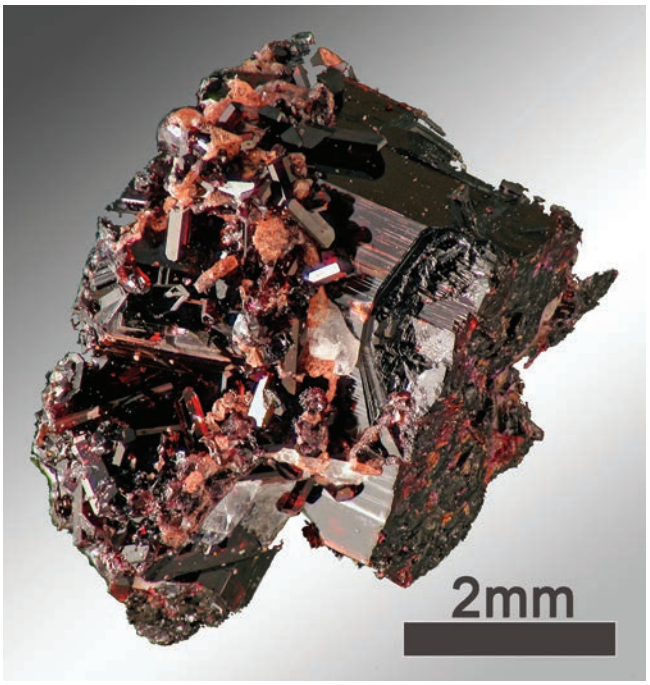

Fig. 1. Cluster of dark red cyprine crystals with minor colourless calcite.

3. General appearance, physical properties and optical data

Cyprine forms chaotic aggregates (up to 5 cm across) of prismatic crystals with lilac hue up to 1-cm long and up to 3-mm thick (Fig. 1). They occur in open cavities or are embedded in a coarse-grained colourless calcite. Cyprine crystals are well-shaped, but typically showing growth-related distortion, with lustrous faces. The dominant form of the prismatic zone is {1 0 0} and the minor is {1 1 0}, both commonly with striations along [0 0 1]; crystals are terminated by the {3 3 1} faces.

Cyprine crystals are dark red with lilac hue and vitreous lustre. Twinning and cleavage are not observed. The Mohs hardness is typical for vesuvianite-group minerals and is equal to 6.5. The density measured by flotation in diluted Clerici solution is 3.40(3) g/cm^3.

The mineral is optically uniaxial, negative, $\omega = 1.744$ (2), $\varepsilon = 1.732(2)$ (in white light) and it displays very strong pleochroism ranging from *O* = dark purple, *E* = pale red to *O* = dark reddish brown, *E* = pale yellowish brown; the absorption scheme is $O \gg E$. The Gladstone–Dale compatibility index (Mandarino, 1981) is −0.038 (excellent; based on the empirical chemical formula).

4. Chemical composition

Chemical analyses were obtained by means of a HITACHI S-3400N scanning-electron-microscope-equipped INCA Wave 500 system (WDS mode; 20 kV; 10 nA: beam diameter 5 μm, 30 s per element). The following standards were used: quartz (Si), corundum (Al), periclase (Mg), calcite (Ca), metallic Mn, goethite (Fe), metallic Cu,

metallic Cr. No elements with $Z > 8$ other than those mentioned above were detected. The H_2O content was determined by thermogravimetric analysis (TGA). Analytical data for two structurally characterized zones [Mg-rich (zone 1) and Mn-rich (zone 2): Figs. 2 and 3] of a cyprine crystal are given in Table 1. The CuO content in the studied samples varies in the range of 1.8–2.5 wt.%, which corresponds to 0.6–1.0 Cu atom per formula unit (apfu). The average of analyses in both zones results in the empirical cyprine formula: $Ca_{19.00}(Cu_{0.81}Mg_{0.19})_{\Sigma 1.00}(Al_{8.33}Mg_{1.64}Mn^{3+}_{1.31}Fe^{3+}_{0.46}Cr_{0.06})_{\Sigma 11.80}Si_{17.88}O_{67.29}(OH)_{10.70}$. The simplified formula is $Ca_{19}Cu^{2+}(Al,Mg,Mn)_{12}Si_{18}O_{69}(OH)_9$.

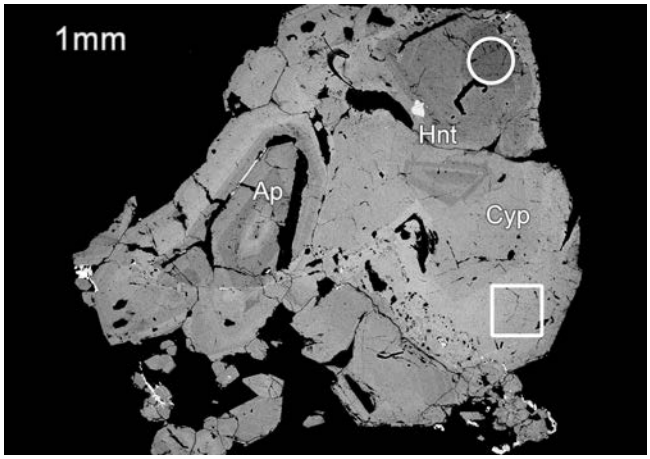

Fig. 2. SEM (BSE) image of near-parallel cluster of cyprine crystals (polished section). White circle shows the Mg-rich zone (microprobe zone-1) and white square shows the Mn-rich zone (microprobe zone-2) used for single-crystal XRD study. Ap – apatite, Hnt – henritermierite, Cyp – cyprine.

5. Powder X-ray diffraction data

Powder X-ray diffraction data (Table 2) were collected by means of a Bruker Phazer D2 diffractometer in the 2θ range of 5–80° (Cu*Kα*; 1.5418 Å) with scanning steps of

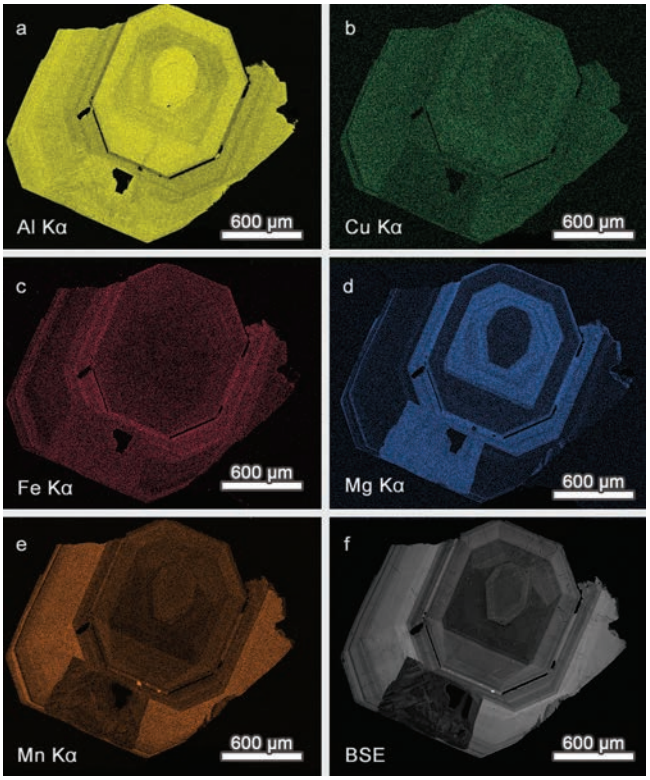

Fig. 3. X-ray distribution maps for Al *Kα* (a), Cu *Kα* (b), Fe *Kα* (c), Mg *Kα* (d), Mn *Kα* (e) radiation and backscattered electron image of a zoned cyprine crystal.

Table 1. Chemical compositions of cyprine in the Mg-rich zone-1 and Mn-rich zone-2.

wt.%	Zone-1-1	Zone-1-2	Zone-1-3	Zone-1-4	Zone-1-5	Zone-1-6	Zone-2-1	Zone-2-2	Zone-2-3
SiO_2	36.85	36.90	37.01	36.88	37.22	36.99	36.54	36.56	36.44
Al_2O_3	15.12	15.21	14.31	14.82	14.61	15.83	13.64	13.73	13.73
CaO	36.48	36.75	36.82	36.71	36.81	36.62	36.28	36.18	36.09
MgO	3.11	3.30	3.57	3.23	3.03	3.21	0.94	1.25	1.13
Mn_2O_3	1.85	2.23	2.55	2.62	2.82	1.56	5.85	6.07	6.22
CuO	2.47	2.12	2.72	2.76	2.36	1.89	1.87	1.77	1.96
Fe_2O_3	0.84	0.55	0.34	0.44	0.72	0.83	2.84	2.54	2.13
Cr_2O_3	0.18	0.25	0.22	0.16	0.33	0.23	0.02	0.04	0.05
H_2O*	3.3	3.3	3.3	3.3	3.3	3.3	3.3	3.3	3.3
Total	100.20	100.61	100.84	100.92	101.20	100.46	101.28	101.44	101.05
Atoms per formula unit normalized on the basis of 19 Ca atoms									
Si	17.91	17.85	17.82	17.82	17.93	17.91	17.86	17.92	17.90
Al	8.66	8.65	8.12	8.44	8.30	9.03	7.86	7.93	7.95
Ca	19.00	19.00	19.00	19.00	19.00	19.00	19.00	19.00	19.00
Mg	2.25	2.37	2.56	2.33	2.18	2.32	0.68	0.91	0.83
Mn	0.68	0.82	0.93	0.96	1.03	0.57	2.18	2.26	2.33
Cu	0.91	0.77	0.99	1.01	0.86	0.69	0.69	0.66	0.73
Fe	0.31	0.20	0.12	0.16	0.26	0.30	1.04	0.94	0.79
Cr	0.07	0.10	0.08	0.06	0.13	0.09	0.01	0.02	0.02
H	10.70	10.62	10.60	10.63	10.60	10.66	10.76	10.79	10.82

* Content of H_2O measured by thermogravimetry analysis (TGA).

Table 2. Powder X-ray diffraction data for cyprine.*

I_{meas}	d_{meas} (Å)	I_{calc}	d_{calc} (Å)	*h k l*	I_{meas}	d_{meas} (Å)	I_{calc}	d_{calc} (Å)	*h k l*
7	9.40	5	9.40	1 0 1	**10**	**2.324**	**8**	**2.323**	**1 4 4**
12	**5.89**	**12**	**5.89**	**0 0 2**	2	2.275	2	2.276	6 3 1
2	5.50	2	5.50	2 2 0	2	2.208	2	2.208	5 3 3
2	5.192	2	5.197	1 1 2	5	2.201	9	2.201	7 1 0
3	4.916	0.3	4.922	3 1 0	1	2.186	3	2.185	7 0 1
5	4.704	5	4.700	2 0 2	2	2.162	5	2.164	7 1 1
3	4.497	0.8	4.499	2 1 2	3	2.141	5	2.141	5 0 4
9	4.019	14	4.023	2 2 2	5	2.122	7	2.121	1 5 4
3	3.886	0.9	3.891	4 0 0	3	2.086	4	2.086	6 2 3
2	3.777	2	3.778	3 1 2	3	2.064	6	2.064	2 5 4
0.6	3.667	0.3	3.668	3 3 0	7	2.042	5	2.044	7 3 0
10	3.482	15	3.480	2 4 0	2	2.026	3	2.027	6 4 2
7	3.244	7	3.248	4 0 2	3	2.014	4	2.014	7 3 1
3	3.073	4	3.072	3 1 3	4	1.9976	6	1.9981	3 6 3
8	3.048	9	3.052	5 1 0	4	1.9635	4	1.9650	6 5 1
12	**3.007**	**12**	**3.010**	**4 3 1**	3	1.9205	3	1.9206	7 1 3
47	**2.950**	**40**	**2.948**	**0 0 4**	10	1.8885	10	1.8892	6 2 4
5	2.906	6	2.906	3 2 3	2	1.7975	2	1.7977	2 8 2
100	**2.752**	**100**	**2.753**	**4 3 2**	8	1.7634	13	1.7638	7 1 4
4	2.666	2	2.669	5 3 0	4	1.7184	2	1.7189	9 1 0
76	**2.594**	**69**	**2.595**	**5 2 2**	**28**	**1.6224**	**25**	**1.6230**	**6 7 2**
5	2.530	3	2.529	3 1 4	5	1.5714	5	1.5723	7 7 0
1	2.498	1	2.501	6 1 1	9	1.5593	8	1.5586	1 6 6
35	**2.459**	**36**	**2.461**	**6 2 0**	2	1.5233	6	1.5222	6 5 5
7	2.441	10	2.440	5 0 3	5	1.4983	4	1.4986	8 4 4
4	2.376	5	2.375	6 0 2	4	1.4753	4	1.4749	5 1 7
7	2.351	5	2.350	4 0 4					

* Eight strongest lines are shown in bold.

0.02°. The normal-focus Cu X-ray tube was operated at 40 kV and 30 mA. Parameters of the tetragonal (space group *P*4/*n*) unit cell obtained by Rietveld refinement using the program Topas (Bruker AXS, 2009) are: $a = 15.5652(5)$ Å, $c = 11.7921(4)$ Å, $V = 2863.2(2)$ Å^3.

6. Crystal structure

Samples extracted from two chemically different zones of a cyprine crystal (Fig. 2) were used for X-ray diffraction experiments carried out using an Agilent Technologies Xcalibur Eos diffractometer, which operated at 50 kV and 40 mA. A hemisphere of three-dimensional data was collected at room temperature using monochromatic Mo*K*α X-radiation for each zone, with frame widths of 1° and 40 s counting time for each frame. Analysis of the reflection dataset indicated *P*4/*n* as the most probable space group for both samples (3 and 23 systematic absence violations have been observed for the reflections 0 *k l* with $k + l \neq 2n$ and *h k l* with $h = k$ and $l \neq 2n$, while 6 and 1 violations of *h k* 0 reflections with $h + k \neq 2n$ are observed (see Armbruster & Gnos, 2000b). A small number of violating reflections is justified by the small difference between the occupation factors of the *Y*1A, *X*4B and *Y*1B, *X*4A positions, which results in the lowering of symmetry from *P*4/*nnc* to *P*4/*n*. The structures were refined to $R_1 = 0.034$ and 0.035 for 2848 and 2071 unique observed reflections with $|F_o| \geq 4\sigma_F$ for zones 1 and 2, respectively, by means of the *SHELX* program (Sheldrick, 2008). Empirical absorption correction was applied in the CrysAlisPro (Agilent Technologies, 2012) program complex using spherical harmonics, implemented in the SCALE3 ABSPACK scaling algorithm. All H atoms were located from the analysis of difference Fourier electron-density maps and were refined with the imposed O–H distance restraints of 0.85 Å. Volumes of coordination polyhedra were calculated using the program VESTA 3 (Momma & Izumi, 2011).

Experimental details are given in Table 3, final atomic coordinates and isotropic displacement parameters in Table 4, selected interatomic distances in Table 5 and parameters of the hydrogen bonding system in Table 6. Anisotropic displacement parameters are freely available in the Supplementary material attached to this article on the GSW website of the journal: http://eurjmin.geoscience world.org/.

In the crystal structure of both crystals of cyprine studied by means of single-crystal X-ray diffraction, the *Z*1A,B; *Z*2A,B and *Z*3A,B sites are almost fully occupied by Si atoms (Fig. 4a). The mean atomic numbers for the *Z*1A,B sites demonstrate small Si deficiencies (site-occupancy factors = 0.94 and 0.97 for the *Z*1A and *Z*1B positions, respectively), in agreement with the substitution scheme $SiO_4^{4-} \leftrightarrow [H_4O_4]^{4-}$ (Galuskin, 2005), which is a typical feature of low-temperature vesuvianites (Armbruster & Gnos 2000a; Galuskin *et al.*, 2003b).

Table 3. Crystal data, data collection and structure refinement parameters for Mg-rich and Mn-rich zones of cyprine.

	Zone-1 (Mg-rich)	Zone-2 (Mn-rich)
Crystal data		
Temperature, diffractometer	293 K, Agilent Technologies Excalibur Eos	
Radiation, wavelength	Mo$K\alpha$, 0.71073 Å	
Crystal system	Tetragonal	
Space group	$P4/n$	
Unit-cell dimensions a, c (Å)	15.5173(4), 11.8230(5)	15.5699(2), 11.8042(2)
Unit-cell volume (Å^3)	2846.8(2)	2861.6(1)
Z	2	2
Calculated density (g/cm^3)	3.44	3.49
Absorption coefficient (mm^{-1})	3.125	3.504
Crystal size (mm^3)	0.15 × 0.14 × 0.12	0.07 × 0.07 × 0.05
Data collection		
2θ range	5.06–57.84°	5.06–53.00°
h, k, l ranges	−20 → 10, −20 → 18, −15 → 15	−18 → 15, −19 → 13, −13 → 14
Total reflections collected	14,877	6688
Unique reflections (R_{int})	3254 (0.028)	2869 (0.037)
Unique reflections $F>4\sigma(F)$	2848	2071
Structure refinement		
Refinement method	Full-matrix least-squares on F^2	
Weighting coefficients a, b	0.0217, 7.1122	0.0096, 0
Data/restraints/parameters	3254/3/320	2869/0/311
R_1 [$F>4\sigma(F)$], wR_2 [$F>4\sigma(F)$]	0.034, 0.077	0.035, 0.070
R_1 all, wR_2 all	0.042, 0.080	0.051, 0.077
Goodness-of-fit on F^2	1.265	0.917
Largest diff. peak and hole, e Å^{-3}	0.43, −0.64	−0.92, 1.49

The X1, X2A,B, X3A,B and X4A,B sites are occupied by Ca atoms only (Fig. 4b). Two eightfold coordinated positions (X4A and X4B) situated within one-dimensional rods have different occupancies: 0.475 and 0.525 for zone-1 and 0.663 and 0.347 for zone-2, respectively.

The main difference between the site-occupancies of the two chemically different zones of cyprine (zone-1 and zone-2) is in the Y-group and X4A,B sites. There is one symmetrically independent Cu site with a square-pyramidal coordination (Panikorovskii *et al.*, 2016a). The Cu-centred polyhedron shows strong Jahn–Teller distortion (Fig. 5): Y1A–O6(4×) = 2.043(3) Å and Y1A–O10 = 2.258(6) Å for zone-1 and Y1B–O6(4×) = 2.010(4) Å and Y1B–O10 = 2.274(7) Å for zone-2. The total mean scattering factor for the Y1A,B site is close to 29 e^-, which indicates that the Y1A,B site is mainly occupied by Cu.

The geometry of the hydrogen bonding system (Table 6) is typical for F-free vesuvianites (Pavese *et al.*, 1998; Lager *et al.*, 1999).

The full crystal-chemical formulae for zone-1 and zone-2 samples of cyprine determined on the basis of crystal-structure refinements can be written as follows: $(Ca)^{X1}{}_{\Sigma2}(Ca)^{X2A}{}_{\Sigma4}(Ca)^{X2B}{}_{\Sigma4}(Ca)^{X3A}{}_{\Sigma4}(Ca)^{X3B}{}_{\Sigma4}(Ca)^{X4A}{}_{\Sigma0.47}(Ca)^{X4B}{}_{\Sigma0.52}(Cu_{0.50}Mg_{0.025})^{Y1A}{}_{\Sigma0.52}(Cu_{0.45}Mg_{0.025})^{Y1B}{}_{\Sigma0.47}(Al)^{Y2A}{}_{\Sigma2}(Al)^{Y2B}{}_{\Sigma2}(Al_{2.80}Mn^{3+}{}_{0.56}Mg_{0.50}Fe^{3+}{}_{0.10}Cr_{0.04})^{Y3A}{}_{\Sigma4}(Al_{2.70}Mn^{3+}{}_{0.63}Mg_{0.50}Fe^{3+}{}_{0.12}Cr_{0.05})^{Y3B}{}_{\Sigma4}(Si_{0.94}[H_4O_4]_{0.06})^{Z1A}{}_{\Sigma1}(Si_{0.97}[H_4O_4]_{0.03})^{Z1B}{}_{\Sigma1}(Si)^{Z2A}{}_{\Sigma4}(Si)^{Z2B}{}_{\Sigma4}(Si)^{Z3A}{}_{\Sigma4}(Si)^{Z3B}{}_{\Sigma4}(O)_{\Sigma69}(OH)_9$ for zone-1 and $(Ca)^{X1}{}_{\Sigma2}(Ca)^{X2A}{}_{\Sigma4}(Ca)^{X2B}{}_{\Sigma4}(Ca)^{X3A}{}_{\Sigma4}(Ca)^{X3B}{}_{\Sigma4}(Ca)^{X4A}{}_{\Sigma0.66}(Ca)^{X4B}{}_{\Sigma0.34}(Cu_{0.30}Mg_{0.037})^{Y1A}{}_{\Sigma0.34}(Cu_{0.60}Mg_{0.063})^{Y1B}{}_{\Sigma0.66}(Al_{1.48}Mn^{3+}{}_{0.40}Fe^{3+}{}_{0.12})^{Y2A}{}_{\Sigma2}(Al_{1.74}Mn^{3+}{}_{0.20}Fe^{3+}{}_{0.06})^{Y2B}{}_{\Sigma2}(Al_{1.90}Mn^{3+}{}_{0.75}Fe^{3+}{}_{0.72}Mn^{2+}{}_{0.40}Mg_{0.22}Cr_{0.01})^{Y3A}{}_{\Sigma4}(Al_{2.82}Mn^{3+}{}_{0.45}Fe^{3+}{}_{0.34}Mn^{2+}{}_{0.20}Mg_{0.18}Cr_{0.01})^{Y3B}{}_{\Sigma4}(Si_{0.94}[H_4O_4]_{0.06})^{Z1A}{}_{\Sigma1}(Si_{0.97}[H_4O_4]_{0.03})^{Z1B}{}_{\Sigma1}(Si)^{Z2A}{}_{\Sigma4}(Si)^{Z2B}{}_{\Sigma4}(Si)^{Z3A}{}_{\Sigma4}(Si)^{Z3B}{}_{\Sigma4}(O)_{\Sigma69}(OH)_9$ for zone-2.

7. TGA/DSC analysis

Thermogravimetry and differential scanning calorimetry (TG/DSC) studies were performed using a NETZSCH STA 449 F3 Jupiter thermoanalyzer in a dynamic argon atmosphere (heating rate: 10 °C/min, with aluminum oxide standard, sample mass 38.2 mg and temperature range with in room temperature to 1100 °C).

Zabinski *et al.* (1996) and Foldvari (2011) studied the dehydroxylation process in vesuvianite and demonstrated the presence of one-step weight losses for most samples in the temperature ranges of 820–1090 and 990–1150 °C, for low- and high-symmetry vesuvianites, respectively. The total values of the reported weight losses matched the OH contents, which did not exceed 9 apfu.

The TGA and DSC curves (Fig. 6) of cyprine have one major step of weight loss, which corresponds to an endothermic effect at 1018 °C and can be assigned to the dehydroxylation of the O(11A,B)H(11A,B) and O(10A,B)H(A,B) groups (Zabinski *et al.*, 1996). Two endothermic

Table 4. Fractional atomic coordinates, displacement parameters (Å^2) and site occupancy for the structure of cyprine.

Site	Zone-1					Zone-2				
	x	*y*	*z*	U_{iso}/U_{eq}	Occupancy	*x*	*y*	*z/c*	U_{iso}/U_{eq}	Occupancy
*Z*1A	1/4	3/4	0	0.0046(7)	Si 0.942(11)	1/4	3/4	0	0.0039(9)	Si 0.946(10)
*Z*1B	3/4	1/4	1/2	0.0067(7)	Si 0.969(11)	3/4	1/4	1/2	0.0047(9)	Si 0.965(10)
*Z*2A	0.68089(6)	0.45926(6)	0.12898(8)	0.00751(19)	Si	0.68159(10)	0.45943(10)	0.13062(10)	0.0105(3)	Si
*Z*2B	0.45930(6)	0.68104(6)	0.37077(8)	0.00738(19)	Si	0.45848(9)	0.68077(10)	0.37213(10)	0.0086(3)	Si
*Z*3A	0.34872(6)	0.41624(6)	0.13498(8)	0.0083(2)	Si	0.34811(9)	0.41400(10)	0.13464(10)	0.0083(3)	Si
*Z*3B	0.41597(6)	0.34874(6)	0.36497(8)	0.0082(2)	Si	0.41745(10)	0.34884(10)	0.36434(10)	0.0082(3)	Si
*X*1	3/4	1/4	0.25008(9)	0.0084(2)	Ca	3/4	1/4	0.25024(10)	0.0072(3)	Ca
*X*2A	0.54365(4)	0.31110(4)	0.12061(6)	0.00834(15)	Ca	0.54471(7)	0.31183(7)	0.12073(7)	0.0075(2)	Ca
*X*2B	0.31112(4)	0.54380(4)	0.37940(6)	0.00832(15)	Ca	0.31081(7)	0.54320(7)	0.37878(7)	0.0075(2)	Ca
*X*3A	0.60100(5)	0.68042(5)	0.11168(7)	0.01342(17)	Ca	0.59908(7)	0.67778(7)	0.11509(8)	0.0130(3)	Ca
*X*3B	0.68009(5)	0.60087(5)	0.38776(7)	0.01337(17)	Ca	0.68077(7)	0.60093(7)	0.39007(8)	0.0125(3)	Ca
*X*4A	1/4	1/4	0.3479(3)	0.0096(9)	Ca 0.475(3)	1/4	1/4	0.3528(2)	0.0093(9)	Ca 0.663(5)
*X*4B	1/4	1/4	0.1519(2)	0.0119(8)	Ca 0.525(3)	1/4	1/4	0.1460(5)	0.0081(17)	Ca 0.337(5)
*Y*2A	1/2	1/2	0	0.0052(3)	Al	1/2	1/2	0	0.0060(5)	Al 0.736(7) + Mn 0.264(7)
*Y*2B	1/2	1/2	1/2	0.0047(3)	Al	1/2	1/2	1/2	0.0069(6)	Al 0.866(7) + Mn 0.134(7)
*Y*3A	0.38891(5)	0.61991(5)	0.12585(7)	0.0072(3)	Al 0.825(5) + Mn 0.175(5)	0.38879(7)	0.61802(7)	0.12502(7)	0.0067(3)	Al 0.528(5) + Mn 0.472(5)
*Y*3B	0.61974(5)	0.38891(5)	0.37396(7)	0.0075(3)	Al 0.803(5) + Mn 0.197(5)	0.62064(8)	0.38878(8)	0.37464(8)	0.0058(4)	Al 0.752(5) + Mn 0.248(5)
*Y*1A	1/4	1/4	−0.5551(2)	0.0123(6)	Cu 0.525(3)	1/4	1/4	−0.5547(3)	0.0062(14)	Cu 0.337(5)
*Y*1B	1/4	1/4	0.05549(18)	0.0101(7)	Cu 0.475(3)	1/4	1/4	0.05286(16)	0.0098(7)	Cu 0.663(5)
O1A	0.28064(15)	0.67262(15)	0.0858(2)	0.0083(5)	O	0.2797(2)	0.6725(2)	0.0858(2)	0.0069(8)	O
O1B	0.67257(15)	0.28057(15)	0.4145(2)	0.0088(5)	O	0.6731(2)	0.2812(2)	0.4147(2)	0.0073(8)	O
O2A	0.65991(15)	0.38220(15)	0.2210(2)	0.0104(5)	O	0.6609(2)	0.3824(2)	0.2230(2)	0.0095(8)	O
O2B	0.38234(15)	0.65996(15)	0.2788(2)	0.0096(5)	O	0.3815(2)	0.6599(2)	0.2803(2)	0.0082(8)	O
O3A	0.45105(15)	0.72188(15)	0.0754(2)	0.0093(5)	O	0.4516(2)	0.7219(2)	0.0749(2)	0.0077(8)	O
O3B	0.72199(15)	0.45100(15)	0.4246(2)	0.0090(5)	O	0.7218(2)	0.4507(2)	0.4251(2)	0.0078(8)	O
O4A	0.60683(15)	0.43767(15)	0.0303(2)	0.0099(5)	O	0.6078(2)	0.4372(2)	0.0320(2)	0.0084(8)	O
O4B	0.43773(15)	0.60683(15)	0.4696(2)	0.0097(5)	O	0.4371(2)	0.6071(2)	0.4714(2)	0.0085(8)	O
O5A	0.32925(15)	0.51429(16)	0.1782(2)	0.0117(5)	O	0.3274(2)	0.5109(2)	0.1783(2)	0.0110(8)	O
O5B	0.51397(16)	0.32904(15)	0.3218(2)	0.0112(5)	O	0.5151(2)	0.3294(2)	0.3212(2)	0.0102(8)	O
O6A	0.27089(16)	0.38036(17)	0.0591(2)	0.0142(5)	O	0.2717(2)	0.3770(2)	0.0564(2)	0.0120(8)	O
O6B	0.37996(17)	0.27087(16)	0.4414(2)	0.0141(5)	O	0.3824(2)	0.2709(2)	0.4406(2)	0.0132(8)	O
O7A	0.67360(15)	0.55614(15)	0.1781(2)	0.0118(5)	O	0.6742(2)	0.5560(2)	0.1803(2)	0.0151(9)	O
O7B	0.55612(15)	0.67387(16)	0.3218(2)	0.0118(5)	O	0.5552(2)	0.6729(2)	0.3239(2)	0.0119(8)	O
O8A	0.43898(15)	0.40857(15)	0.0667(2)	0.0092(5)	O	0.4384(2)	0.4075(2)	0.0654(2)	0.0076(8)	O
O8B	0.40845(15)	0.43869(15)	0.4340(2)	0.0095(5)	O	0.4087(2)	0.4392(2)	0.4322(2)	0.0073(8)	O
O9	0.35485(15)	0.35480(15)	0.2498(2)	0.0112(5)	O	0.3554(2)	0.3531(2)	0.2504(2)	0.0087(8)	O
O10A	3/4	3/4	0.3641(5)	0.0146(11)	O	3/4	3/4	0.3634(5)	0.0147(17)	O
O10B	3/4	3/4	0.1360(5)	0.0135(11)	O	3/4	3/4	0.1398(5)	0.0172(17)	O
O11A	0.49504(16)	0.56201(16)	0.1359(2)	0.0099(5)	O	0.4939(2)	0.5616(2)	0.1380(2)	0.0084(8)	O
O11B	0.56196(16)	0.49479(16)	0.3641(2)	0.0097(5)	O	0.5624(2)	0.4951(2)	0.3630(2)	0.0084(8)	O
H11A	0.508(4)	0.526(4)	0.186(5)	0.07(2)	H					
H11B	0.533(4)	0.507(4)	0.305(4)	0.050	H					
H10B	3/4	3/4	0.220(7)	0.01(2)	H					

Table 5. Selected interatomic distances (Å) for the crystal structure of cyprine.

Bond	Zone-1	Zone-2		Bond	Zone-1	Zone-2	
*Z*1A–O1A	1.642(2)	1.642(3)	×4	*X*3A–O10B	2.567(1)	2.621(1)	
				*X*3A–O7B	2.582(3)	2.558(3)	
*Z*1B–O1B	1.640(2)	1.640(3)	×4	*X*3A–O8A	2.596(3)	2.577(3)	
				*X*3A–O6A	2.987(3)	2.982(3)	
*Z*2A–O7A	1.616(2)	1.619(4)		⟨*X*3A–O⟩	2.556	2.560	
*Z*2A–O3A	1.641(2)	1.645(4)					
*Z*2A–O2A	1.649(2)	1.652(3)		*X*3B–O7B	2.365(3)	2.384(4)	
*Z*2A–O4A	1.672(3)	1.672(3)		*X*3B–O3B	2.453(2)	2.460(4)	
⟨*Z*2A–O⟩	1.645	1.647		*X*3B–O11B	2.480(3)	2.493(4)	
				*X*3B–O6B	2.480(3)	2.456(3)	
*Z*2B–O7B	1.614(3)	1.615(4)		*X*3B–O7B	2.495(3)	2.512(4)	
*Z*2B–O3B	1.639(2)	1.643(4)		*X*3B–O10A	2.571(1)	2.5784(14)	
*Z*2B–O2B	1.648(2)	1.650(3)		*X*3B–O7A	2.576(3)	2.574(3)	
*Z*2B–O4B	1.675(3)	1.674(3)		*X*3B–O8B	2.590(3)	2.595(3)	
⟨*Z*2B–O⟩	1.644	1.646		*X*3B–O6B	2.985(3)	2.456(3)	
				⟨*X*3B–O⟩	2.555	2.501	
*Z*3A–O6A	1.604(3)	1.611(4)					
*Z*3A–O8A	1.621(2)	1.630(4)		*X*4A–O6B	2.324(3)	2.336(4)	×4
*Z*3A–O5A	1.633(3)	1.625(4)		*X*4A–O9	2.576(3)	2.592(3)	×4
*Z*3A–O9	1.661(3)	1.667(3)		⟨*X*4A–O⟩	2.450	2.464	
⟨*Z*3A–O⟩	1.630	1.633					
				*X*4B–O6A	2.325(3)	2.275(4)	×4
*Z*3B–O6B	1.609(3)	1.605(4)		*X*4B–O9	2.576(3)	2.602(4)	×4
*Z*3B–O8B	1.621(2)	1.624(4)		⟨*X*4B–O⟩	2.451	2.439	
*Z*3B–O5B	1.633(3)	1.632(4)					
*Z*3B–O9	1.662(3)	1.657(3)		*Y*2A–O11A	1.875(2)	1.893(3)	×2
⟨*Z*3B–O⟩	1.631	1.630		*Y*2A–O8A	1.879(2)	1.896(3)	×2
				*Y*2A–O4A	1.952(2)	1.980(3)	×2
*X*1–O1A	2.333(3)	2.331(3)	×2	⟨*Y*2A–O⟩	1.902	1.923	
*X*1–O1B	2.334(3)	2.332(3)	×2				
*X*1–O2A	2.506(2)	2.506(3)	×2	*Y*2B–O11B	1.875(2)	1.888(3)	×2
*X*1–O2B	2.507(2)	2.508(3)	×2	*Y*2B–O8B	1.879(2)	1.887(3)	×2
⟨*X*1–O⟩	2.420	2.419		*Y*2B–O4B	1.952(2)	1.964(3)	×2
				⟨*Y*2B–O⟩	1.902	1.913	
*X*2A–O8A	2.309(2)	2.319(4)					
*X*2A–O5A	2.327(2)	2.330(4)		*Y*3A–O11A	1.880(3)	1.864(4)	
*X*2A–O3A	2.375(2)	2.369(3)		*Y*3A–O2B	1.915(2)	1.948(3)	
*X*2A–O2A	2.425(2)	2.435(3)		*Y*3A–O1A	1.928(2)	1.954(3)	
*X*2A–O5B	2.439(3)	2.426(3)		*Y*3A–O3A	1.946(2)	1.980(4)	
*X*2A–O4A	2.441(2)	2.423(3)		*Y*3A–O5A	1.981(3)	2.024(4)	
*X*2A–O1A	2.490(2)	2.482(3)		*Y*3A–O4A	2.052(3)	2.044(3)	
*X*2A–O6A	2.927(3)	3.010(4)		⟨*Y*3A–O⟩	1.950	1.969	
⟨*X*2A–O⟩	2.467	2.474					
				*Y*3B–O11B	1.875(2)	1.893(4)	
*X*2B–O8B	2.315(2)	2.312(4)		*Y*3B–O2A	1.915(3)	1.900(3)	
*X*2B–O5B	2.325(2)	2.326(4)		*Y*3B–O1B	1.931(2)	1.921(4)	
*X*2B–O3B	2.374(3)	2.372(3)		*Y*3B–O3B	1.951(2)	1.943(4)	
*X*2B–O2B	2.426(2)	2.419(3)		*Y*3B–O5B	1.984(3)	1.990(4)	
*X*2B–O5A	2.439(3)	2.434(3)		*Y*3B–O4B	2.054(3)	2.027(3)	
*X*2B–O4B	2.440(2)	2.459(3)		⟨*Y*3B–O⟩	1.952	1.946	
*X*2B–O1B	2.488(2)	2.514(3)					
*X*2B–O6B	2.936(3)	2.898(4)		*Y*1A–O6B	2.043(3)	2.091(4)	×4
⟨*X*2B–O⟩	2.468	2.467		*Y*1A–O10A	2.259(6)	2.260(7)	
				⟨*Y*1A–O⟩	2.086	2.125	
*X*3A–O7A	2.367(2)	2.356(4)					
*X*3A–O3A	2.452(2)	2.443(4)		*Y*1B–O6A	2.049(3)	2.010(4)	×4
*X*3A–O6A	2.476(3)	2.525(3)		*Y*1B–O10B	2.264(6)	2.274(7)	
*X*3A–O11A	2.482(3)	2.454(4)		⟨*Y*1B–O⟩	2.094	2.063	
*X*3A–O7A	2.496(2)	2.521(4)					

Table 6. Selected interatomic distances (Å), angles (°) and distances between nearest anions for hydrogen bonds in the structure of cyprine (zone-1).

d(*D*–H)	*d*(H*A*)	*d*(*DA*)	∠*D*H*A*	Bond
0.850	2.318	3.073	148.24	O11A–H11AO11B
0.850	2.235	3.073	168.47	O11B–H11BO11A
0.987	1.699	2.687	179.97	O10B–H10BO10A

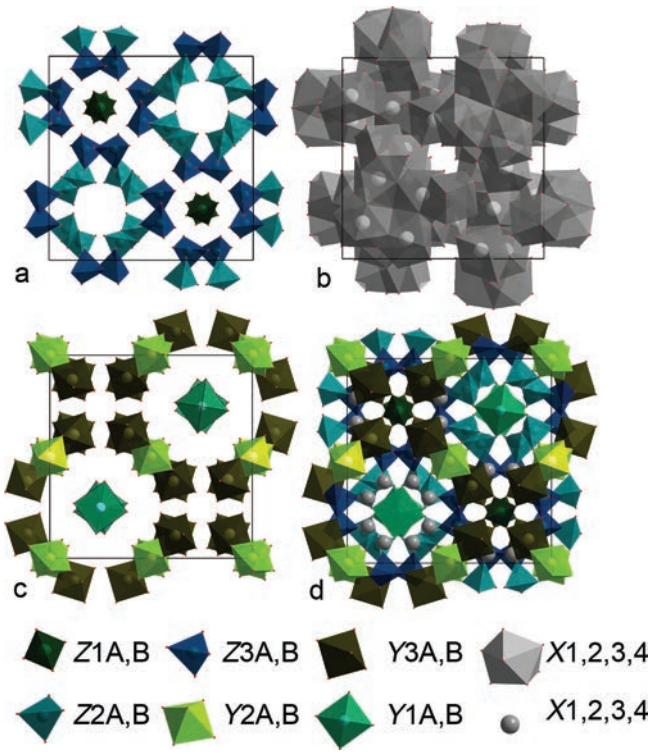

Fig. 4. The crystal structure of cyprine projected along the *c* axis. (a) Arrangement of *Z*-cation polyhedra: green, green-blue, dark blue represent *Z*1A,B; *Z*2A,B and *Z*3A,B tetrahedra, respectively; (b) arrangement of the *X*-cation polyhedra: grey polyhedra, grey spheres represent polyhedra and atoms of Ca; (c) arrangement of the *Y*-cation polyhedra: light green and dark green octahedra are of the *Y*2A,B and *Y*3A,B positions; green square pyramids are of the *Y*1A, B sites occupied by Cu; (d) the overall crystal structure.

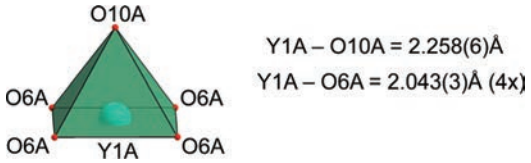

Fig. 5. Square-pyramidal coordination of Cu^{2+} in the crystal structure of cyprine zone-1.

peaks at 850–900 and 972 °C may correspond to the disappearance of $(H_4O_4)^{4-}$ groups (Panikorovskii *et al.*, 2016b) or separated dehydroxylation of OH arranged at the rods and assigned to the O10A,B positions. The total weight loss for cyprine is 3.30 %, which is in good agreement with a theoretical H_2O content of 3.10 %.

8. Infrared spectroscopy

The IR spectrum (Fig. 7) was collected at room temperature by means of a Bruker Vertex 70 IR spectrometer (cyprine powder in KBr pellet, 4 cm^{-1} resolution). The absorption band at 443 cm^{-1} belongs to the v_2 symmetric bending vibrations of the Si–O bonds. The absorption band at 490 cm^{-1} belongs to the $[Me–O]_6$ vibrations. The bands at 574, 604 and the shoulder at 671 cm^{-1} correspond to the v_4 asymmetric bending vibrations of the Si–O bonds. The bands at 814, 905, 972 and 1015 cm^{-1} may be assigned to asymmetric stretching vibrations of the Si–O and Si–O–Si bonds. The presence of a doublet with equal intensities of its components (574 and 604 cm^{-1}) corresponding to the v_4 asymmetric bending vibrations indicates, according to Kurazhkovskaya *et al.* (2003), *P*4/*n* symmetry.

The bands in the range 3354–3640 cm^{-1} correspond to O–H stretching vibrations. The sharp 3640 cm^{-1} band corresponds to the ***B*** band (3635) according to Groat *et al.* (1995) and is characteristic for the Al–Al–OH environment of the O11(A,B) hydroxyl position. The intense broad band at 3354 cm^{-1} most likely corresponds to the Cu–OH configuration of O10A,B–H sites (this band was absent in the IR spectra measured by Groat *et al.*, 1995).

9. Optical absorption spectra

Polarized, room-temperature optical absorption spectra in the range 270–1100 nm (37,037–9091 cm^{-1}) were recorded on doubly polished single-crystal sections at a spectral resolution of 1 nm using an AVASPEC-ULS2048 × 16 spectrometer attached *via* a 400-μm UV fibre cable to a Zeiss Axiotron UV-microscope. A 75-W Xenon arc was used as a light source and Zeiss Ultrafluar 10× lenses served as objective and condenser. The size of the circular measurement aperture was 64 μm in diameter. A UV-quality Glan-Thompson prism with a working range from 250 to 2700 nm (40,000 to 3704 cm^{-1}) was used as polarizer. The wavelength scale of the spectrometer was calibrated against Ho_2O_3 doped and Pr_2O_3/Nd_2O_3 doped standards (Hellma glass filters 666F1 and 666F7).

The polished sections of crystal fragments selected from the microprobe zones 1 and 2 (Fig. 2) were 46-μm thick. They were cut perpendicular to the crystallographic *a*-axis allowing measurements in $\mathbf{E} \parallel E$ (*i.e.* ∥ the *c*-axis) and $\mathbf{E} \parallel O$). Spectra were measured on untreated crystal slabs as well as after subsequent heat treatment at 600 °C in H_2 atmosphere. The treated samples were placed in a gold container and pushed into a preheated horizontal tube furnace equipped with a quartz-glass tube. The heating experiment lasted for 8 h and was terminated by pushing the samples out to the cold zone of the quartz tube.

The optical absorption spectra recorded on untreated polished crystal fragments from microprobe zone-1 and zone-2 is shown in Fig. 8a. Spectra of the zone-1 fragment show absorption bands with bandwidths (~2000 cm^{-1}) typical for spin-allowed electronic *d*–*d* transitions at

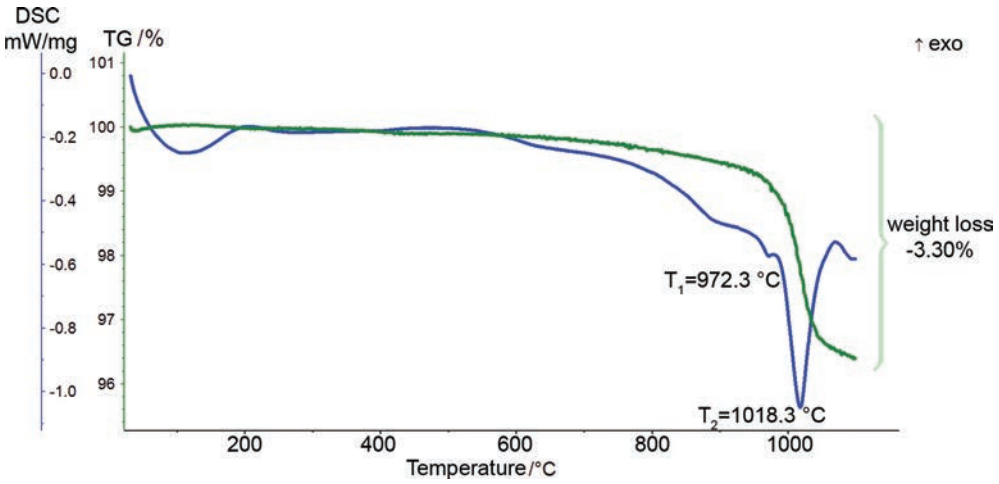

Fig. 6. Thermogravimetric weight loss (wt.%, green line) and differential scanning calorimetry (blue line) curves of cyprine.

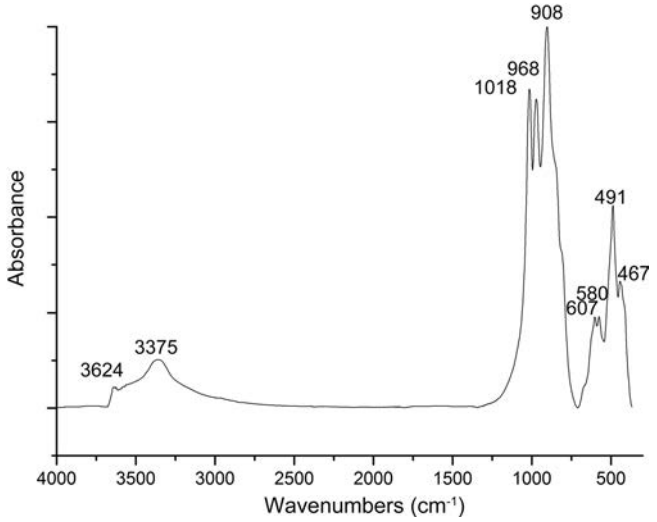

Fig. 7. Infrared spectrum of cyprine.

23,500, 21,800, 15,400 and 12,000 cm^{-1}. In addition, weaker narrow bands with widths (<800 cm^{-1}) typical for spin-forbidden electronic *d–d* transitions are observed at 21,100 and 20,000 cm^{-1}. The spectra of the zone-2 crystal fragment is dominated by a very strong and broad (width >3500 cm^{-1}) absorption band at 24,000 cm^{-1}, which occurs in addition to those observed in the spectra of the zone-1 crystal fragment. With the exception of the band at 23,500 cm^{-1}, all the observed absorption bands in spectra of the untreated crystals are strongly polarized in **E** || *O*. Apart from the appearance of the 15,400 cm^{-1}, the recorded cyprine spectra show strong resemblances to those of Cu-free, Mn-rich vesuvianite crystals from Lower Silesia, Poland, which were interpreted in terms of spin-allowed electronic *d–d* transitions in five- and six-coordinated Mn^{3+} (Platonov *et al.*, 1995).

Spectra recorded on the zone-1 and zone-2 crystal fragments after heat treatment in H_2 atmosphere show strong decrease in intensity of the major absorption bands at 18,000 and 12,000 cm^{-1}. The intensities of the minor narrow bands at 21,100 and 20,000 cm^{-1} also decrease. The intensities of the absorption bands at 15,400 and 24,000 cm^{-1} are unaffected or nearly so by the heat treatment under reducing conditions (Fig. 8b).

In accordance with the results of a spectroscopic study on copper-bearing low-Mn vesuvianite from Sauland, Norway (Dyrek *et al.*, 1992), we assign the 15,400 cm^{-1} band to a spin-allowed *d–d* transition in five-coordinated Cu^{2+} at the *Y*1-site. The absorption bands at 23,500, 21,100, 20,000, 18,000 and 12,000 cm^{-1} that decrease in intensity on crystal treatment under reducing conditions are assigned to spin-forbidden and spin-allowed *d–d* transitions in octahedrally coordinated Mn^{3+} at the *Y*3 site. The intense and broad absorption band observed at 24,000 cm^{-1} in **E** || *O* spectra of crystal fragment 2 is assigned, on the basis of its band width, polarization and lack of response to treatment under reducing conditions in combination with the determined cation occupancies, to a pair band absorption involving Mn^{2+} and Mn^{3+} at *Y*2 and *Y*3 sites. Comparable intensification and broadening of Mn^{2+}-related electronic transitions have previously been recorded in spectra of phlogopite (Smith *et al.*, 1983) and spinel (Hålenius & Bosi, 2014) and assigned to electronic transitions in exchange coupled pairs of transition metal cations.

10. Discussion

Striation on the prism faces along [0 0 1] (Fig. 1) is typical for the *P*4/*n* vesuvianites indicating intergrowth of domains with variable ordering in the channel-like rods parallel to the *c*-axis and hence slightly variable symmetry (Armbruster & Gnos, 2002; Gnos & Armbruster, 2006). In the absence of high amounts of Fe or moderate amounts of Mn, cyprine would probably have blue to blue-green pleochroism due to Cu^{2+} (Dyrek *et al.*, 1992). However, as can be seen in our case, less than 2 wt.% of Mn_2O_3 is already sufficient to overtone the blue colour, resulting in red to lilac pleochroism.

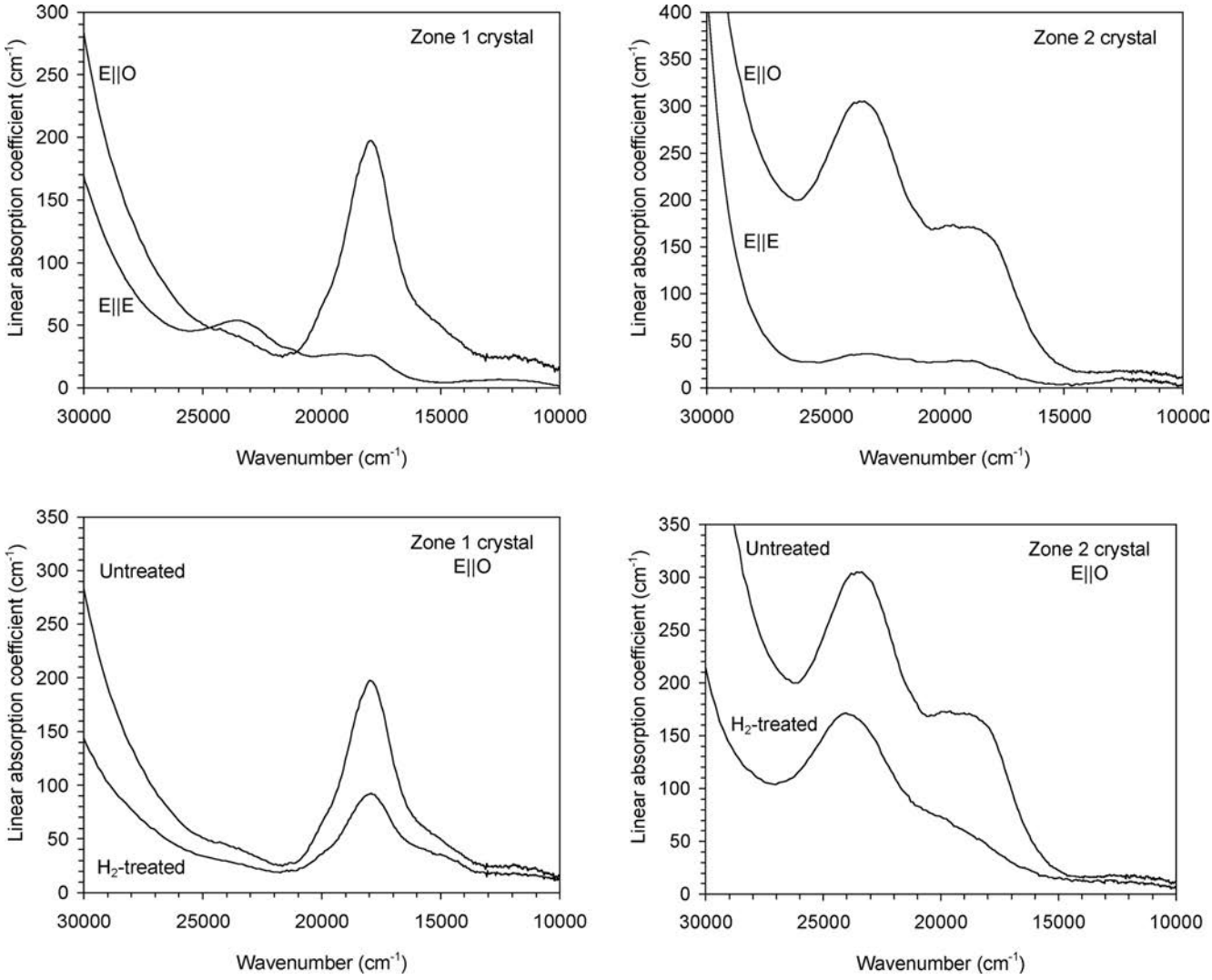

Fig. 8. Polarized optical absorption spectra of cyprine from zones 1 and 2 (top) and **E** || *O* spectra of the same crystals before and after heat-treatment in reduced (H_2) atmosphere (bottom).

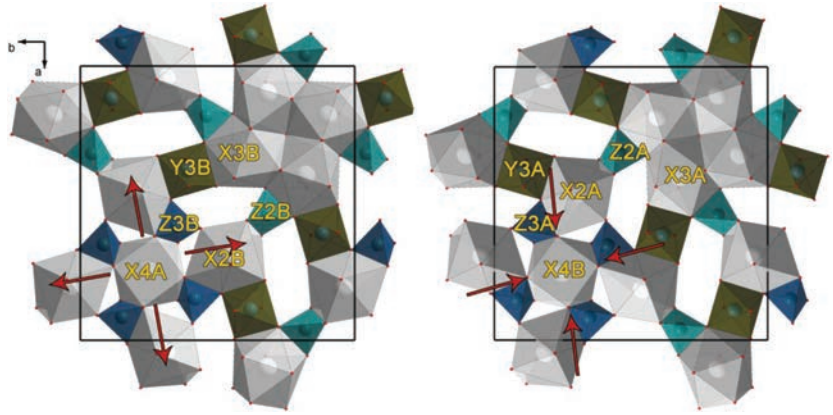

Fig. 9. Polyhedral sheet in the crystal structure of the zone-2 cyprine grain at different levels along the *c* axis: (a) $z = 0.85$; (b) $z = 0.65$; red arrows show tension direction as a result of different occupations of the Ca4A,B positions.

In agreement with the optical absorption spectra, the zone-2 contains some Mn in a divalent state. As in the previous crystal-structure refinement of low-symmetry Mn-rich vesuvianites and manganvesuvianite from the Kalahari manganese field (Armbruster & Gnos, 2000a), Mn^{2+}/Fe^{2+} were located in the *Y*3A, *Y*3B sites, corroborated by the mean ⟨*Y*3A,B–O⟩ bond length being longer than the ⟨*Y*2A,B–O⟩ bond length (Table 5). On the

Table 7. Comparative data of polyhedral volumes at zone-1 and zone-2 of cyprine (Å^3).

Polyhedron	Zone-1	Zone-2
*Z*1A	2.2553	2.2576
*Z*1B	2.2483	2.2511
*Z*2A	2.2580	2.2664
*Z*2B	2.2553	2.2612
*Z*3A	2.2187	2.2317
*Z*3B	2.2240	2.2165
*X*1	24.4005	24.3687
*X*2A	24.2017	24.6890
*X*2B	24.6316	24.6657
*X*3A	32.8884	33.0575
*X*3B	32.8277	33.0976
*X*4A	24.2017	24.4278
*X*4B	24.1588	24.0449
*Y*1A	6.3930	6.7344
*Y*1B	6.4560	6.2402
*Y*2A	9.0836	9.3897
*Y*2B	9.0823	9.2243
*Y*3A	9.8019	10.1063
*Y*3B	9.8220	9.7326
Total	251.4088	253.2632

basis of redox potential arguments, Fe^{2+} is incompatible with Mn^{3+}, and consequently, we conclude that Mn^{2+} is the only divalent transition metal cation present in addition to Cu^{2+} in our cyprine. Armbruster & Gnos (2000a) and Armbruster *et al.* (2002) reported different occupancies by Mn and Fe of the *Y*3A–*Y*3B pair (Al2a and Al2b in Armbruster & Gnos, 2000a) for the *P*4/*n* vesuvianite, which is in contrast to Kurazhkovskaya *et al.* (2003) and Galuskin *et al.* (2007), who distinguish between 'low' (*P*4/*n* and *P*4*nc*) and 'high' (*P*4/*nnc*) vesuvianites by the various occupancies of only the *X*4A, B and *Y*1A,B sites. Different population of these sites is associated with the cation ordering inside the structural rods (Armbruster & Gnos, 2000c; Galuskin *et al.*, 2007). The increase in size of the *X*4A square antiprism (occupancy $Ca_{0.66}$ and $V = 24.43$ Å^3) leads to increasing tension in the polyhedral sheet (Fig. 9c) and induces compression of the *Y*3B octahedra (occupancy $Al_{0.75}Mn_{0.25}$ and $V = 9.73$ Å^3). The respective compression of the *X*4B (Fig. 9b) polyhedra (occupancy $Ca_{0.34}$ and $V = 24.05$ Å) is compensated by the expansion of the *Y*3A polyhedra (occupancy $Al_{0.52}Mn_{0.48}$ and $V = 10.11$ Å^3) associated with the $Al^{3+} \leftrightarrow Mn^{3+}$ substitution.

It is of interest that the unit-cell parameters of the Mg-rich zone-1 ($a = 15.5173(4)$ Å, $c = 11.8230(5)$ Å) and the Mn-rich zone-2 ($a = 15.5699(2)$ Å, $c = 11.8042(2)$ Å) observed in cyprine are significantly different. Comparison of the volumes of cation polyhedra in the crystal structure of both zones (Table 7) demonstrates that the most significant change is observed for the *Y*2A,B and *Y*3A,B octahedra, as a result of $Mg^{2+} + Al^{3+} \leftrightarrow Fe^{3+} + Mn^{2+}$ substitution.

Acknowledgements: This work was supported by Russian Science Foundation (grant 14-17-00071). Experimental studies were carried out using resources of the X-ray Diffraction Centre and Geo Environmental Centre "Geomodel" of Saint-Petersburg State University. The authors are grateful to Gregory Yu. Ivanyuk for the photograph of the cyprine specimen.

References

Agilent Technologies (2012): CrysAlisPro, Version 1.171.36.20 release 27-06-2012.

Allen, F.M. & Burnham, C.W. (1992): A comprehensive structure-model for vesuvianite: symmetry variations and crystal growth. *Can. Mineral.*, **30**, 1–18.

Armbruster, T. & Gnos, E. (2000a): *P*4/*n* and *P*4*nc* long range ordering in low-temperature vesuvianites. *Am. Mineral.*, **85**, 563–569.

—, — (2000b): Tetrahedral vacancies and cation ordering in low-temperature Mn-bearing vesuvianites: indication of hydrogarnet-like substitution. *Am. Mineral.*, **85**, 570–577.

—, — (2000c): "Rod" polytypism in vesuvianite: crystal structure of a low-temperature *P*4*nc* with pronounced octahedral cation ordering. *Schweiz. Mineral. Petrogr. Mitt.*, **80**, 109–116.

Armbruster, T., Gnos, E., Dixon, R., *et al.* (2002): Manganvesuvianite and tweddillite, two new Mn^{3+}-silicate minerals from the Kalahari manganese fields, South Africa. *Mineral. Mag.*, **66**, 137–150.

Bellatreccia, F., Cámara, F., Ottolini, L., Della Ventura, G., Cibin, G., Mottana, A. (2005):Wiluite from Ariccia, Latium, Italy: occurrence and crystal structure. *Can. Mineral.*, **43**, 1457–1468.

Berzelius, J.J. (1821): Die Anwendung des Löthrohrs in der Chemie und Mineralogie, 263 p.

Britvin, S.N., Antonov, A.A., Krivovichev, S.V., Armbruster, T., Burns, P.C., Chukanov, N.V. (2003): Fluorvesuvianite, $Ca_{19}(Al, Mg,Fe^{2+})_{13}[SiO_4]_{10}[Si_2O_7]_4O(F,OH)_9$, a new mineral species from Pitkäranta, Karelia, Russia: description and crystal structure. *Can. Mineral.*, **41**, 1371–1380.

Cairncross, B., Beukes, N., Gutzmer, J. (1997): The manganese adventure – the South African manganese fields. Associated Ore & Metal Corporation Limited, Johannesburg, Republic of South Africa, 236 p.

Coda, A., Giusta, D.A., Isetti, G., Mazzi, F. (1970): On the structure of vesuvianite. *Atti Acad. Sci. Torino*, **105**, 1–22.

Dixon, R.D. (1989): Sugilite and associated metamorphic silicate minerals from Wessels mine, Kalahari manganese field. *S. Afr. Geol. Surv. Bull.*, **93**, 47.

Dyrek K., Platonov A.N., Sojka Z., Zabinski W. (1992): Optical absorption and EPR study of Cu^{2+} ions in vesuvianite ("cyprine") from Sauland, Telemark, Norway. *Eur. J. Mineral.*, **4**, 1285–1289.

Fitzgerald, S, Rheingold, A, Leavens, P. (1986a): Crystal structure of a Cu-bearing vesuvianite. *Am. Mineral.*, **71**, 1011–1014.

—, —, — (1986b): Crystal structure of a non-*P*4/*nnc* vesuvianite from Asbestos, Quebec. *Am. Mineral.*, **71**, 1483–1488.

Foldvari, M. (2011): Handbook of thermogravimetric system of minerals and its use in geological practice. Geological Institute of Hungary ed., Budapest, 180 p.

Galuskin, E.V. (2005): Minerals of vesuvianite group from achtarandite rocks (Wiluy River, Yakutia). University of Silesia, Katowice, Poland, 191 p. (in Polish).

Galuskin, E.V., Galuskina, I.O., Sitarz, M., Stadnicka, K. (2003a): Si-deficient, OH-substituted, boron-bearing vesuvianite from the Wiluy River, Yakutia, Russia. *Can. Mineral.*, **41**, 833–842.

Galuskin, E.V., Armbruster, T., Malsy, A., Galuskina, I.O., Sitarz, M. (2003b): Morphology, composition and structure of low-temperature *P*4/*nnc* high-fluorine vesuvianite whiskers from Polar Yakutia, Russia. *Can. Mineral.*, **41**, 843–856.

Galuskin, E.V, Galuskina, I.O, Stadnicka, K., Armbruster, T., Kozanecki M. (2007): The crystal structure of Si-deficient, OH-substituted, boron-bearing vesuvianite from the Wiluy River, Sakha – Yakutia, Russia. *Can. Mineral.*, **45**, 239–248.

Giuseppetti, G. & Mazzi, F. (1983): The crystal structure of a vesuvianite with *P*4/n symmetry. *Tschermaks Mineral. Petrogr. Mitt.*, **31**, 277–288.

Gnos, E. & Armbruster, T. (2006): Relationship among metamorphic grade, vesuvianite "rod polytypism", and vesuvianite composition. *Am. Mineral.*, **91**, 862–870.

Gnos, E., Armbruster, T., Villa, I.M. (2003): Norrishite, $K(Mn_2^{3+}Li)Si_4O_{10}(O)_2$, an oxymica associated with sugilite from the Wessels Mine, South Africa: crystal chemistry and ^{40}Ar–^{39}Ar dating. *Am. Mineral.*, **88**, 189–194.

Groat, L.A., Hawthorne, F.C., Ercit T.S. (1992): The chemistry of vesuvianite. *Can. Mineral.*, **33**, 19–48.

Groat, L.A., Hawthorne, F.C., Rossman, G.R., Scott T.E. (1995): The infrared spectroscopy of vesuvianite in the OH region. *Can. Mineral.*, **33**, 609–626.

Groat, L.A., Hawthorne, F.C., Ercit, T.S., Grice, J.D. (1998): Wiluite, $Ca_{19}(Al,Mg,Fe,Ti)_{13}(B,Al,\square)_5Si_{18}O_{68}(O,OH)_{10}$, a new mineral species isostructural with vesuvianite, from the Sakha Republic, Russian Federation. *Can. Mineral.*, **36**, 1301–1304.

Hålenius, U. & Bosi, F. (2014): Color of Mn-bearing gahnite: a first example of electronic transitions in heterovalent exchange coupled $^{IV}Mn^{2+}$-$^{VI}Mn^{3+}$ pairs in minerals. *Am. Mineral.*, **99**, 261–266.

Kleyenstuber, A.S.E. (1984): The mineralogy of the manganese bearing Hotazel formation of the Proterozoic Transvaal sequence of Griqualand West, South Africa. *Trans. Geol. Soc. S. Afr.*, **87**, 257–272.

Krivovichev, S.V. (2013): Structural complexity of minerals: information storage and processing in the mineral world. *Mineral. Mag.*, **77**, 275–326.

Kurazhkovskaya, V.S., Borovikova, E. Yu., Dorokhova, G.I., Kononov, O.V., Stefanovich, S. Yu. (2003): IR spectra of high-symmetric and low symmetric vesuvianites. *Proc. RMS*, **132**, 109–121 (in Russian).

Lager, G.A., Xie, Q., Ross, F.K., et al. (1999): Hydrogen-atom position in *P*4/*nnc* vesuvianite. *Can. Mineral.*, **37**, 763–768.

Lindström, G. (1890): Analyses of idocrase. *Geol. Fören. Förh.*, **10**, 287.

Machatschki, F. (1932): Zur Formel des Vesuvian. *Z. Kristallogr.*, **81**, 148–152.

Mandarino, J.A. (1981): The Gladstone-Dale relationship: Part IV. The compatibility concept and its application. *Can. Mineral.*, **19**, 441–450.

Momma, K. & Izumi, F. (2011): VESTA 3 for three-dimensional visualization of crystal, volumetric and morphology data. *J. Appl. Crystallogr.*, **44**, 1272–1276.

Ohkawa, M., Yoshiasa, A., Takeno, S. (1992): Crystal chemistry of vesuvianite: site preferences of square-pyramidal coordinated sites. *Am. Mineral.*, **77**, 945–953.

Panikorovskii, T.L., Zolotarev Jr. A.A., Krivovichev, S.V., Shilovskikh, V.V., Bazai A.V. (2016a): Crystal chemistry of Cu-bearing vesuvianites ("cyprine") from Kleppan (Norway). *Proc. RMS*, **145**, 131–142 (in Russian).

Panikorovskii, T.L., Krivovichev, S.V., Galuskin, E.V., Shilovskikh, V.V., Mazur, A.S. (2016b): Si-deficient, OH-substituted, boron-bearing vesuvianite from Sakha-Yakutia, Russia: a combined single-crystal, ^1H MAS-NMR and IR spectroscopic study. *Eur. J. Mineral.*, **28**, 931–941. DOI:10.1127/ejm/2016/0028-2570.

Pavese, A., Prencipe, M., Tribaudino, M., Aagaard, S.S. (1998): X-ray and neutron single-crystal study of *P*4*/n* vesuvianite. *Can. Mineral.*, **36**, 1029–1037.

Platonov, A.N., Zabinski W., Sachanbinski, M. (1995): Optical absorption spectra of Mn^{3+} ions in vesuvianites from Lower Silesia, Poland. *Eur. J. Mineral.*, **7**, 1345–1352.

Shannon, E.V. (1922): Note on the cyprine from Franklin Furnace, New Jersey. *Am. Mineral.*, **7**, 140–142.

Sheldrick, G.M. (2008): A short history of SHELX. *Acta Crystallogr. A*, **64**, 112–122.

Smith, G., Hålenius, U., Annersten, H., Ackermann, L. (1983): Optical and Mössbauer spectra of manganese-bearing phlogopites: Fe_{IV}^{3+}-Mn_{VI}^{2+} pair absorption as the origin of reverse pleochroism. *Am. Mineral.*, **68**, 759–768.

Topas (2009): General profile and structure analysis software for powder diffraction data. Version 4.2. Bruker AXS GmbH, Karlsruhe, Germany.

Warren, B.E. & Modell, D.I. (1931): The structure of vesuvianite $Ca_{10}Al_4(Mg,Fe)_2Si_9O_{34}(OH)_4$. *Z. Kristallogr.*, **78**, 422–432.

Werner, A.G. (1795): Über Vsuvian. *Klaproth's Beiträge*, **1**, 34.

Zabinski, W., Wactawska, Z., Paluszkiewicz, C. (1996): Thermal decomposition of vesuvianite. *J. Therm. Anal.*, **46**, 1437–1447.

Received 26 May 2016
Modified version received 18 August 2016
Accepted 19 August 2016